Eur. Phys. J. A (2022) 58:209
https://doi.org/10.1140/epja/s10050-022-00861-0

THE EUROPEAN PHYSICAL JOURNAL A

Regular Article - Experimental Physics

Gamma-ray cross-sections of the ^{27}Al(p,p'γ)^{27}Al reaction in the proton energy range 1490–3000 keV

R. Mateus[1,a], **M. Fonseca**[2,3,4], **J. Cruz**[2,3], **V. Manteigas**[2], **C. Santos**[2], **H. Luís**[5], **H. Silva**[2], **A. P. Jesus**[2,3]

[1] DECN, Instituto Superior Técnico, Universidade de Lisboa, 2695-066 Bobadela, Portugal
[2] LIBPhys-Laboratory of Instrumentation, Biomedical Engineering and Radiation Physics, 2829-516 Caparica, Portugal
[3] NOVA School of Science and Technology, NOVA University Lisbon, Campus Caparica, 2829-516 Caparica, Portugal
[4] HEI-Lab: Digital Human-Environment Interaction Lab, Lusófona University, Lisbon, Portugal
[5] IPFN, Instituto Superior Técnico, Universidade de Lisboa, 2695-066 Bobadela, Portugal

Received: 4 July 2022 / Accepted: 12 October 2022 / Published online: 29 October 2022

Communicated by Aurora Tumino.

Abstract The ^{27}Al(p,p'γ)^{27}Al nuclear reaction provides the highest cross-sections for gamma-ray emission in aluminium. As a result, the corresponding γ_1—844 keV and γ_2—1014 keV gamma lines are commonly used for gamma-ray technique analysis of Al in solid samples. In this work, we report a detailed measurement of the excitation functions for both gamma-ray emissions performed with a HPGe detector placed at an angle of 130º. All the resonances are described in detail by using small energy steps for the incident proton beam from 1490 to 3000 keV, revealing new energy levels of ^{28}Si. Cross-sections data are validated by comparing experimental values of gamma-ray yields of pure thick Al samples with those calculated by the ERYA-Bulk code, confirming the accuracy of the measurements. Cross-sections and thick target yields obtained in this work are compared with other published data.

1 Introduction

During the last sixty years, analytical techniques based on accelerated ion beams have established a firm ground of reference techniques for a multitude of problems pertaining to various domains, ranging from material science and technology to geology, archaeometry, biomedical sciences and environment.

An effort has been made to measure and compile necessary parameters to provide these techniques with quantitative potentialities [1, 2]. To do so, measurement of the cross-section events is mandatory when they cannot be calculated easily, as in the case of Rutherford backscattering.

Despite the high sensitivity of Proton Induced Gamma-Ray Emission (PIGE) for light elements detection, PIGE has remained till recent years as a semi-quantitative technique based on a comparative study with standards (homogeneous thick samples of known composition) [2], which commonly have elemental compositions different from the samples under analysis. A consequence of the procedure is a distinct energy loss imposed by both compositions (samples under analysis and standards) to the incident ion beams, and the nature of the involved PIGE cross-sections enhances analytical issues, as nuclear reaction excitation functions are rarely smooth, displaying narrow and large resonances. However, we have shown that, if cross-sections are available in numerical values at energy steps close enough to define in detail the resonances, trivial integration leads to elemental concentrations [3–5]. This methodology becomes, as for the case of general ion beam analytical techniques, standard free, transforming PIGE into a primary reference technique. The code we have developed, the ERYA-Bulk code [3–5], integrates the relevant nuclear reaction cross-sections along the depth of the samples to obtain isotopic gamma-ray yields. Knowing the natural abundance of each isotope, elemental contents arise from quantification. First results justified the importance of a methodology to develop PIGE, which starts by measuring the correspondent cross-sections of relevant gamma-producing nuclear reactions. An effort has been made within an IAEA concerted project to compile, evaluate and measure relevant cross-sections [6]. Nevertheless, the experimental results remain scarce, and most of them measured generally with wide energy steps [6, 7].

[a] e-mail: rmateus@ctn.tecnico.ulisboa.pt(corresponding author)

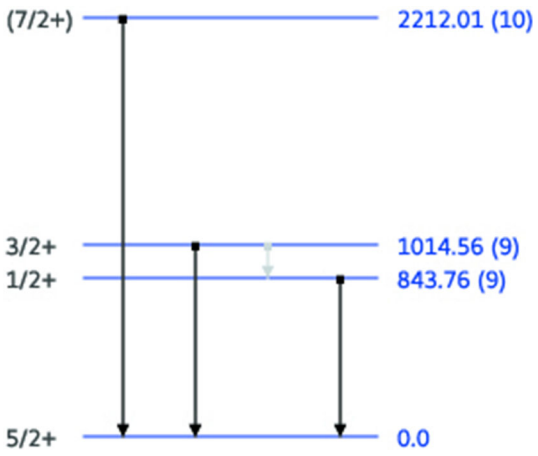

Fig. 1 Levels of ^{27}Al (from LiveCharts of Nuclides, IAEA [9])

This work reports the activity performed in our laboratory to measure in detail the excitation functions of gamma emissions with the highest yields, providing the best sensitivity for the quantification of Al by PIGE; i.e., the γ_1—844 keV and γ_2—1014 keV lines arising from the inelastic scattering of protons by ^{27}Al, the ^{27}Al(p,p'γ)^{27}Al reaction [2]. The lines arise from transitions of the first and second excited states to the ground state of ^{27}Al (see Fig. 1) [8–10]. Regarding the difference in energy of both lines, we may anticipate the same difference for the corresponding threshold energies enabling gamma emission, meaning that γ_1 emission channel opens at slightly lower incident energies (~ 160 keV), for the proton beams, than γ_2. The transition γ_3 of 2212 keV will occur also. However, it will be only significant at very high incident energy beams and therefore it is not so important for Al quantification. The first and second excited states of ^{27}Al have total angular momenta of $1/2^+$ and $3/2^+$ (Fig. 1), respectively, and therefore we expect an isotropic behaviour for the γ_1—844 keV emission and a possible anisotropy for γ_2—1014 keV [11].

Other gamma-rays of higher energy are produced during the bombardment of ^{27}Al by proton capture, i.e., ^{27}Al(p,γ)^{28}Si (the energy of the first excited state of ^{28}Si is 1779 keV [1, 2]). However, the process has a much smaller cross-section than for inelastic scattering. Additionally, gamma-ray detector efficiency decreases at higher detection energies, and therefore inelastic scattering leads to much higher sensitivities for general analytical purposes. In opposition and for depth-profiling analysis, radiative proton capture exhibits several very narrow and rather isolated resonances, which have been intensely used for that purpose [1, 2]. A third nuclear reaction occurs simultaneously, the ^{27}Al(p,$\alpha\gamma$)^{24}Mg reaction, but the produced 1369 keV gamma-ray (the energy of the first excited state of ^{24}Mg) may also be obtained by bombardment of Na and Mg by protons via ^{23}Na(p,γ_1)^{24}Mg and ^{24}Mg(p,p'γ_1)^{24}Mg [1, 2]. Therefore, it is not suitable for analytical purposes, unless one is sure that sodium and magnesium are not present in the sample.

A direct way to validate the experimental cross-sections is to use them for the calculus of the gamma-ray yields induced by the incidence of proton beams on (thick) standards, and to check the calculated results with corresponding experimental values.

Additionally, nuclear cross-section measurements provide important information about the compound nuclei. In the present experiment, the experimental resonant energies of the induced gamma lines, described in the laboratory system, $E_R \equiv (E_R)_{LAB}$, are compared to the energy levels of the ^{28}Si compound nucleus above the energy formation threshold given by ^{27}Al + p (11,585 keV), described in the centre of mass system, (E-level) $\equiv$ (E-level)$_{CM}$, and available from nuclear databases [8–10]. The exercise enabled us to check if all the ^{28}Si levels populated by the ^{27}Al(p,p'γ)^{27}Al were previously reported [8–10].

2 Experiment

This work was carried out at Laboratory of Accelerators and Radiation Technologies (LATR) of Instituto Superior Técnico (IST), Portugal, in two different experimental beam lines [12] with energy resolutions of 1 keV, as measured from the 1779 keV gamma-ray emission of the ^{27}Al(p,γ)^{28}Si reaction at the 992 keV resonant energy (resonant width $\Gamma_R \approx$ 0.07 keV) [1, 2]. Proton beams with energies up to 2.4 MeV were generated at the 2.5 MV Van de Graaff accelerator. The beam energy was calibrated from the analysing magnet field measured by an NMR magnetometer, making use of the 340.5 keV, 872.1 keV and 1373.2 keV resonant energies of ^{19}F(p,$\alpha\gamma$)^{16}O, and also the 1645.1 keV and 1930.7 keV resonances of ^{23}Na(p,p'γ_1)^{23}Na reactions. Ion currents reaching the reaction chamber were kept under 250 nA in order to avoid pile-up events. The employed beam line and experimental chamber were previously described [13].

Measurements with proton energies ranging from 2.0 up to 3.0 MeV where done with the 3.0 MV Tandem accelerator [12] using beam currents close to 100 nA. The energy calibration made use of the 1645.1 keV and 1930.7 keV resonances of ^{23}Na(p,p'γ_1)^{23}Na and of the 3470 keV resonance of ^{16}O(p,p)^{16}O. A 90º analysing magnet and a 25º switching magnet lead the beam to the reaction chamber, passing through several electromagnetic optical devices focusing and steering the beam. Ion trajectory is defined with three aperture systems and the beam current intensity can be monitored by four Faraday cups before reaching the chamber. Apart from two modifications, the reaction chamber was the same used in the Van de Graaff accelerator. A new collimator electrically insulated was developed to further inhibit gamma-background radiation, starting by a nickel foil (1 cm

diameter aperture, 2 mm thickness), followed by a gold foil (2 mm aperture, 1 mm thickness) and finally by a stainless-steel foil (2 mm of aperture, 1 mm thickness). The entire chamber electrically insulated from the beam line and pump system, including a sampler holder and a beam stopper (to avoid the collection of backscattered ions in particle spectra from the chamber wall), is operated as a Faraday cup for charge collection [14].

Gamma-ray spectra were collected by a HPGe detector positioned at an angle of 130º to the beam direction having a relative efficiency of 45% and an energy resolution of 2.2 keV for the 1.173 MeV gamma decay line of ^{60}Co. The detector absolute efficiency was determined by means of ^{133}Ba and ^{152}Eu radioactive sources (with emission energies from 81 keV to 1.5 MeV) located at the target position, and calibrated in activity with an uncertainty of 5%. For the collection of the 844 keV and 1014 keV events, the absolute efficiency is 5.76×10^{-3} and 5.01×10^{-3}, respectively. Backscattered particles were detected by a Passivated Implanted Planar Silicon (PIPS) detector with an intrinsic efficiency ε_p of 100% and energy resolution of 15 keV (for the detection of 5.49 MeV alphas emitted from a ^{241}Am source), placed inside a metal box with an aperture diameter of 6 mm, and electrically insulated from it, at an angle of 165° to the beam direction. The particle detection geometry [13, 14] assures a solid angle of 3.65 msr within an uncertainty of 2.3%.

Cross-section measurements made use of a thin Al layer evaporated on self-supporting and pre-evaporated silver (Ag) thin film. The sample was characterized by Rutherford Backscattering Spectrometry (RBS) using a 1770 keV ^{4}He$^+$ ion beam towards the Al layer, leading to thicknesses of $(1.6 \pm 0.1) \times 10^{17}$ at/cm^2 (7.2 ± 0.5 μg/cm^2) for the Al film and of $(8.0 \pm 0.1) \times 10^{17}$ at/cm^2 (143.3 ± 1.8 μg/cm^2) for the Ag one. The atomic ratio r between Al and Ag contents in the sample is of 0.20 (see Eq. 3). The value was achieved from the area of both Al and Ag particle yields in the RBS spectra. Figure 2 presents one of the collected spectra during characterization. The energies signalizing the presence of each element at the surface of the Al layer are identified with vertical dash lines. Al is in the top layer and Ag is part of a second and deeper one, while the corresponding backscattering yield is recoiled to lower energies. The same behaviour shows that carbon (C) and oxygen (O) are present as contaminants in the Ag film. In the Al film, only few amounts of O exist. The influence of C and O contamination in the cross-section measurement is negligible in face of the layer's thickness and imposed energy loss corrections. The experiment was carried out in the proton energy range 1490–3000 keV by impinging the proton beam on the Al layer. At the end, the validation of the entire excitation functions was done with the ERYA-Bulk code [5] using the corresponding cross-section data as input files to calculate thick target gamma-ray yields

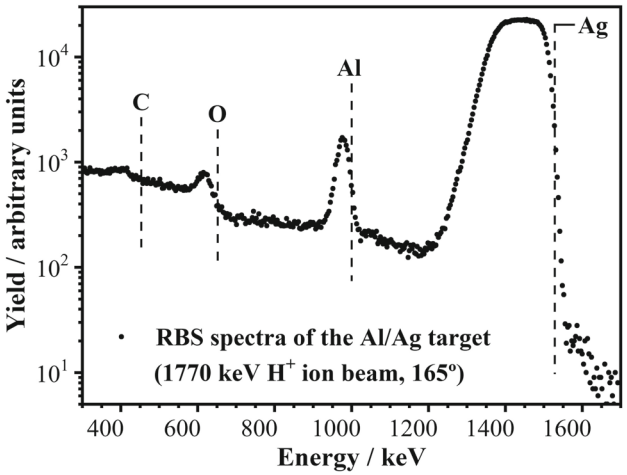

Fig. 2 RBS spectra collected from the Al/Ag target with a 1770 keV H^+ ion beam impinging the Al film at a scattering angle of 165º

[5]. Corresponding experimental and calculated thick target yields were compared.

2.1 Cross-section measurements and validation

When gamma rays are induced from off-resonant energies or from on-resonances larger than the target energy width, the gamma-ray radiation yield Y_γ emitted from the Al thin film and collected within a small solid angle Ω, is given by:

$$Y_\gamma(E, \theta) = \sigma(E, \theta) N_p N_i 4\pi \varepsilon_{\gamma, abs} \quad (1)$$

Here, N_p is the number of incident protons, N_i is the number of i nuclei in the target per surface unit (^{27}Al nuclei in the present case), $\varepsilon_{\gamma, abs}$ is the absolute efficiency of the gamma detector at the energy of the emitted gamma rays, and $\sigma(E, \theta)$ is the nuclear reaction cross-section we are looking for at the incident laboratory energy E and detection laboratory angle θ.

The methodology used to measure the cross-sections also relies on the Rutherford backscattering yield induced by the heavy component in the target, i.e., the Ag self-supporting film. The number of protons elastically scattered by Ag at an angle β, inside a small solid angle, is calculated by:

$$Y_{Ag}\left(E', \beta\right) = \sigma_{R, Ag}(E', \beta) N_p N_{Ag} \Omega_p \varepsilon_p \quad (2)$$

where N_{Ag} is the number of Ag nuclei in the target per surface unit, Ω_p and ε_p are respectively the solid angle and the intrinsic efficiency of the particle detector and $\sigma_{R, Ag}(E', \beta)$ is the Rutherford cross-section at the laboratory energy E' and scattering laboratory angle β related to the elastic scattering of protons by Ag nuclei.

Table 1 Predicted uncertainties for the experimental results

Random	
γ-ray peak area (statistics and area determination)	2%
Proton (Ag) peak area (statistics and area determination)	1%
Overall random uncertainty	2%
Systematic	
γ-ray detector efficiency	5%
Proton detector solid angle	3%
Ratio of Al to Ag	6%
Overall systematic uncertainty	8%

If r is the ratio between the N_i number of i nuclei (^{27}Al nuclei) and of Ag nuclei in the self-supporting thin target, we may write, using expressions (1) and (2) that

$$\sigma(E,\theta) = \frac{\sigma_{R,Ag}\left(E',\beta\right)Y_\gamma(E,\theta)\Omega_p\varepsilon_p}{rY_{Ag}\left(E',\beta\right)\Omega\varepsilon_{\gamma,int}} \quad (3)$$

This way, the large uncertainties associated to the measurement of the absolute number of incident protons (beam charge collection) is avoided. Variables E and E' refer to the effective energies inducing gamma-ray emission and particle scattering in both Al and Ag films, respectively (see text below).

Table 1 presents the predicted uncertainties of the cross-section results, where a separation between random and systematic uncertainties is made.

In relation to deviations caused by gamma-ray anisotropy, we have to state that although the solid angle of the gamma-ray detector is large, encompassing an angular detection range, of ± 30° around 130°, the detector is placed near the angular position of 125°, the neutral angle related to a cos^2 dependence of the angular distribution for gamma emission, which is the expected main component of the angular dependence for alignment [2, 11]. Also, from previous measurements [11] no large anisotropy is expected (please see discussion).

The final excitation functions do not arise directly from the experimental gamma-ray yields, while the thickness of the Al target imposes a correction to the incident proton beam energy. For non-resonant energies or when the resonance width is larger or of the order of the (energy) width of the Al target, ΔE, the incident proton beam energy E_0 is typically corrected to an *effective energy* "$E_{eff} = E_0 - \Delta E/2$", i.e., a correction is imposed to the energy scale in the excitation function [15]. In the present work, and due to the low energy thickness of the Al target used for the present experiment (~ 1.6×10^{17} at/cm^2; ~ 7.2 μg/cm^2), only slight energy corrections varying from 0.49 to 0.30 keV for incident proton energies ranging from 1490 to 3000 keV are imposed,

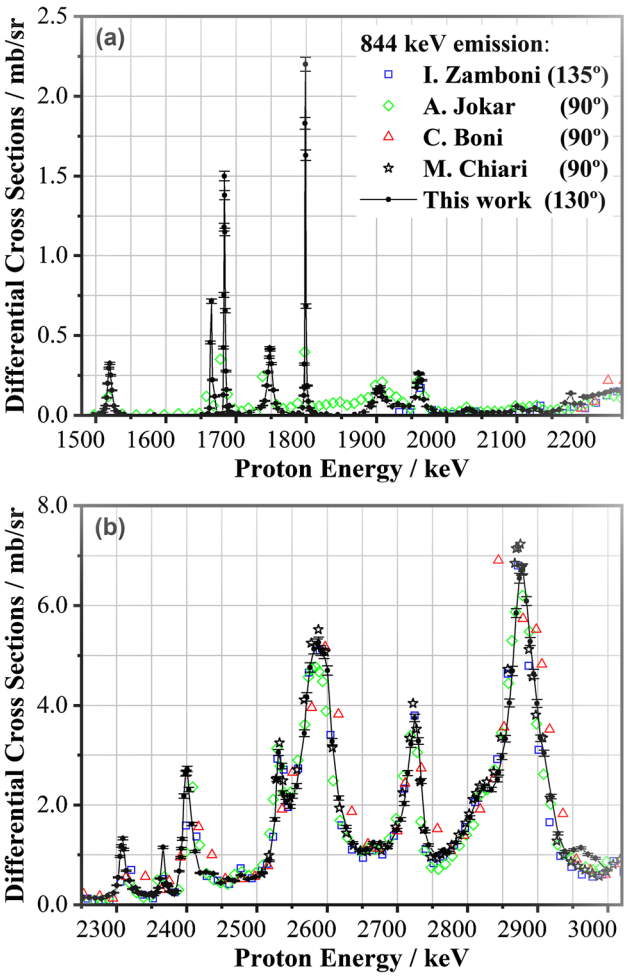

Fig. 3 Differential cross-sections of the ^{27}Al(p,p'γ$_1$)^{27}Al emission at the proton energy ranges of 1.49–2.25 MeV (**a**) and of 2.25–3.00 MeV (**b**)

respectively, while the corresponding energy losses calculated for the impinging protons within the Al lattice decrease from 0.97 keV down to 0.60 keV [16]. The excitation functions graphically presented in Figs. 3 and 4 in Sect. 3 take into consideration the slight corrections. A different approach was carried out at thinner resonances observed at lower incident energies, as referred below.

Some resonances of the excitation functions of ^{27}Al(p,p'γ)^{27}Al reactions have natural widths smaller than the energy thickness of the target. Then Eq. 1 is no longer valid, while gamma yields are obtained from the integral of the cross-section through the thickness of the target ΔE, taking into consideration the corresponding energy loss, $S(E)$, of the projectiles.

$$Y_\gamma(E,\theta) = 4\pi\varepsilon_{\gamma,abs}N_pN_i\int_{E-\Delta E}^{E}\sigma(E,\theta)/S(E)dE \quad (4)$$

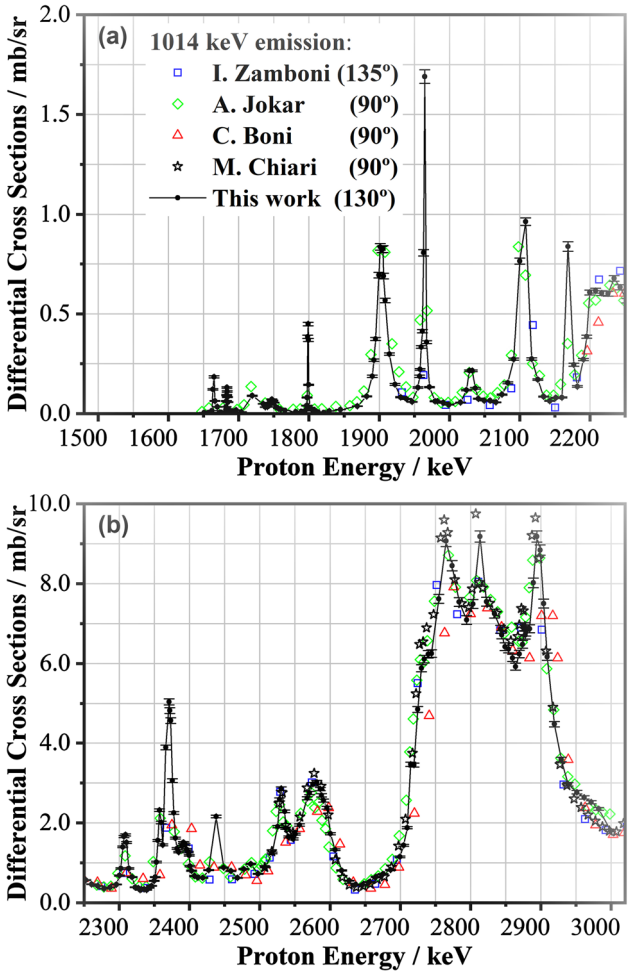

Fig. 4 Differential cross-sections of the ^{27}Al(p,p'γ_2)^{27}Al emission at the proton energy ranges of 1.49–2.25 MeV (**a**) and of 2.25–3.00 MeV (**b**)

Hence, from the procedure described above with Eqs. 1, 2 and 3, one does not obtain "true" cross-section values. In order to determine "true resonances parameters" as the resonant energy E_R, resonant energy width Γ_R and the resonant cross-section σ_R, Breit-Wigner fits were done to the experimental resonant yields, where $\sigma(E,\theta)$ is given by the Breit-Wigner formula depending on E_R, Γ_R and σ_R [15, 17]:

$$\sigma(E,\theta) = \sigma_R \frac{E_R}{E} \frac{\Gamma_R^2}{4(E-E_R)^2 + \Gamma_R^2} \tag{5}$$

Additional information about the fitting procedure involving also the energy spread of the incident beam by straggling effect through the Al layer is given elsewhere [17].

The ERYA-Bulk code calculates gamma-ray yields for homogeneous thick targets with Eq. 6 by following the energy loss of the impinging ions along the depth of the sample and the corresponding cross-sections $\sigma(E,\theta)$, being E_0 the energy of the incident ion beam [3–5]:

$$Y_\gamma(E_0,\theta) = 4\pi\varepsilon_{\gamma,abs} N_p f_m f_i N_{av} A^{-1} \int_0^{E_0} \sigma(E,\theta)/S_m(E)dE \tag{6}$$

Most of ion beam analysis applications make use of mass units. Equation 6 explicits the elemental mass fraction f_m from the elemental atomic volume density n_i, $n_i = f_m \cdot f_i \cdot N_{av} \cdot A^{-1} \cdot \rho$, where A, f_m and f_i are the atomic mass, elemental mass fraction and isotopic abundance of the element under analysis and corresponding isotope i, respectively (in the present case it refers to Al and ^{27}Al), N_{av} is the Avogadro's number and ρ is the mass density of the target. In Eq. 6, ρ is part of the integrand function, converting the energy loss imposed to the ions along the target's depth x into a mass stopping power $S_m(E)$ [2, 3, 5, 16]. In Eq. 1, N_i relates with n_i by $N_i = n_i \cdot x$. The calculus of the integral divides the sample' surface in n sublayers parallel to the surface boundary, i.e., the energy range of the incident ions is divided in n energy intervals were the stopping power may be taken as constant [3, 5]. In each iterative step a stopping power $S_m(E)$ and an energy loss ΔE are calculated [16], leading to a precise incident proton energy with corresponding cross-section value $\sigma(E,\theta)$ arising from the excitation function [3, 5]. These values are used to calculate a gamma-ray yield induced in each sublayer as: $S_m(E)^{-1} \int_{E-\Delta E}^{E} \sigma(E'',\theta)dE''$.

3 Results and discussion

Excitation functions achieved in this work for the γ_1 – 844 keV and γ_2 – 1014 keV lines are presented in Figs. 3 and 4 (see the numerical forms in the IBANDL database for a standard free PIGE analysis [7]). Cross-section were measured along 268 distinct incident proton energies, defining in detail the existing resonances. Additional cross-sections available from I. Zamboni et al. (within the 1930–3050 keV energy range) [6], A. Jokar et al. (in the 1500–3000 keV energy range) [18], C. Boni et al. (1930–3800 keV energy range) [19] and M. Chiari (2500–4090 keV energy range) [20] for the same emissions are shown.

There is a good agreement among the measured data for incident energies above 2.5 MeV. Nevertheless, the magnitude of resonant yields differs from different authors, and it becomes evident from the comparison of all the data that it also exists a proton energy deviation of 5–20 keV among them. For measurements made with a large energy step where care to define the resonance maxima was not taken, the referred energy deviation turns the comparison among authors only indicative. From 2.5 to 3.0 MeV, the measurements agree within the experimental uncertainty at both on

and off resonance. Below 2.5 MeV, the energy steps of Zamboni et al. [6] and Jokar et al. [18] are too large, missing most of the resonances. At some large features of the excitation function, their results agree with the ones measured in this work, within the experimental uncertainty. Boni et al. [19] miss most of the resonances due to the very large step employed. Nevertheless, between resonances their values agree with the other values including the ones of this work, within the experimental uncertainty. Energy shifts close to 5 keV exist at higher incident proton energies between our results and the ones of Chiari et al. [20]. In resume, although a fair good agreement between cross-section values available from different authors in the energy range 2.5–3.0 MeV, the measurements carried out in the present work led to a detailed knowledge of both excitation functions. Most of all, small energy steps in the incident energy beam lead to new and detailed description of the resonant energies and magnitudes for resonances in the energy range 1.5–2.5 MeV.

We may also evaluate the angular distribution for both γ_1 – 844 keV and γ_2—1014 keV emissions by comparing the cross-sections data available from different authors at distinct detection geometries: at 45º [20] (not included in Figs. 3 and Fig. 4), 90º [18–20], 130º (this work) and at 135º [6]. The γ_1—844 keV emission is expected to present an isotropic angular distribution, while it is originated by a j = 1/2 level (Fig. 1) [11], and the isotropic behaviour is observed in Fig. 3. Therefore, the differential cross-section per solid angle unit may be determined in a straightforward way. The same does not apply to the γ_2—1014 keV line coming from a j = 3/2 level [11]. Nevertheless, one may verify that all the cross-section data collected at 90º, 130º and 135º and shown in Fig. 3 follow the same trend. Also Chiari et al. have obtained results at 45° for this line, which are equal, within the experimental uncertainty to the ones obtained at 90° [20], meaning that if any anisotropic behaviour is present in the γ_2 emission, it is likely to be rather small [11].

The excitation functions measured in this work and presented graphically in Figs. 3 and 4 were used for validation as input data of the ERYA-Bulk code considering a pressed pellet of $AlTiO_5$ as target material [5]. Calculated and experimental gamma yields measured with the pellet at different incident proton energies were converted afterwards to pure Al, by using the corresponding stopping powers [16] and Al concentrations (see Eq. 4). Figure 5 compares these results with other experimental thick target yields for the γ_1—844 keV line measured for pure Al by Jokar [21], Deconnink [22], Chiari [23], Kiss [24] and Antilla [25]. Calculated (this work) and experimental thick target yields for the 1014 keV line, also for pure Al and measured in this work and by Jokar [21], Deconnink [22], Chiari [23], Kiss [24] and Savidou [26] are shown in Fig. 6. Depending on the resonant energies (E_R) and resonant energy widths (Γ_R) present in the excitation function of both γ_1—844 keV and

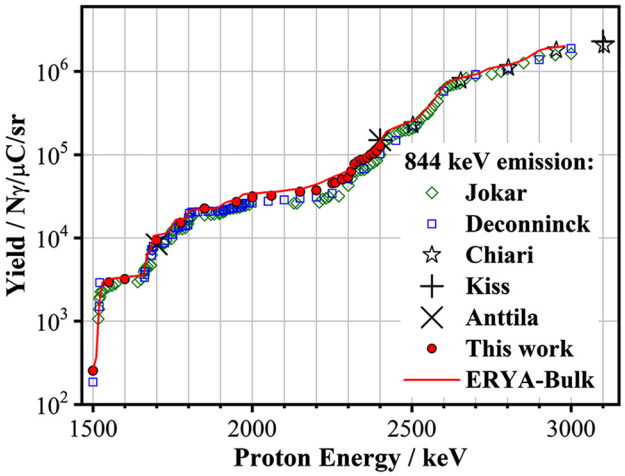

Fig. 5 Calculated gamma-ray yields for the reaction $^{27}Al(p,p'\gamma)^{27}Al$ (γ_1—844 keV)

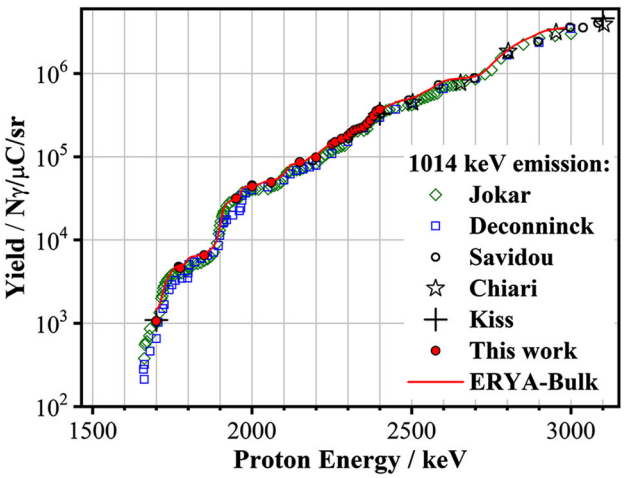

Fig. 6 Calculated gamma-ray yields for the reaction $^{27}Al(p,p'\gamma)^{27}Al$ (γ_2—1014 keV)

γ_2—1014 keV emissions, gamma-ray yields induced in bulk materials increase with incident proton energy. In order to compare all the data along a wide energy range where bulk yields differ by orders of magnitude, semi-logarithmic plots are used.

In relation to thick target yields of the 844 keV gamma line, the agreement of measured and calculated yields is better than 20%, within the uncertainty range. Enhanced deviations are only present in the energy region from 2100 to 2300 keV, where Jokar [21] and Deconninck [22] values, not increasing as they should, reach a deviation of around 50% in relation to the ERYA curve.

For the 1014 keV line the ERYA curve is around 20% higher than Jokar [21] and Deconninck [22] yields and 5 to 10% higher than the yields measured by the other authors [23, 24, 26], within the uncertainty range. There is an exception

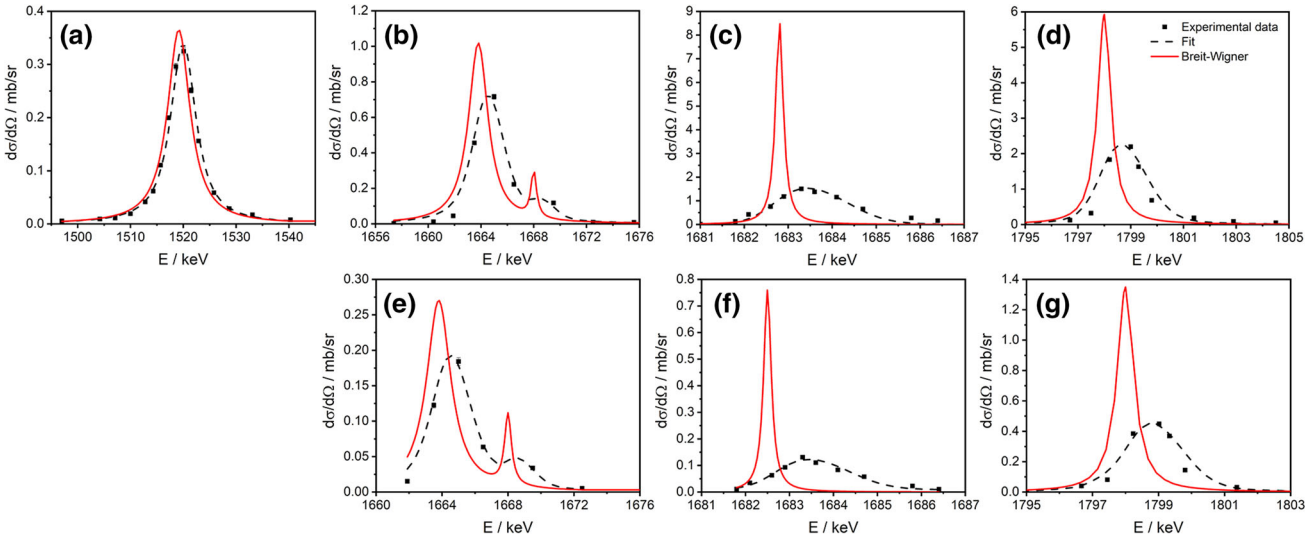

Fig. 7 Experimental cross-sections of ^{27}Al(p,p'γ)^{27}Al thin resonances (black squares), fits achieved from the integration of the experimental points (dashed curves) and true Breit-Wigner resonances (red curves). 1519 keV (**a**), 1664 and 1668 keV (**b**), 1683 keV (**c**) and 1798 keV resonances of γ_1—844 keV (**d**); 1664 and 1668 keV (**e**), 1683 keV (**f**) and 1798 keV resonances of γ_2—1014 keV (**g**)

Table 2 Breit-Wigner parameters for very thin resonances of ^{27}Al(p,p'γ)^{27}Al (resonant energies E_R, energy widths Γ_R, cross-sections σ_R). Uncertainties relate to the fitting procedure [15]

E_R (keV)	Γ_R (keV)	σ_R—844 keV (mb/sr)	σ_R—1014 keV (mb/sr)
1519.2 ± 0.1	5.18 ± 0.05	0.37 ± 0.02	-
1663.8 ± 0.1	1.80 ± 0.05	1.02 ± 0.04	0.27 ± 0.01
1668.0 ± 0.1	0.50 ± 0.06	0.26 ± 0.08	(1.00 ± 0.05) × 10^{-1}
1682.8 ± 0.1	0.21 ± 0.03	8.59 ± 0.16	0.76 ± 0.05
1798.0 ± 0.1	0.60 ± 0.04	5.93 ± 0.19	1.35 ± 0.08

for the small energy region from 1900 to 1960 keV, where Deconninck [22] values are around 50% lower than the ERYA curve, being the other experimental values very close to the ERYA curve.

Concerning the relation between ERYA calculated thick target yields using our cross-section data, and the thick target yields measured in this work, we have results for the 844 keV line and for the 1014 keV line which are 10% and 3% lower than the calculated ones. It is not unexpectable that a deviation may occur between calculated and measured yields since the measured ones depend on the absolute value of the beam collected charge, while cross section values are independent of this quantity. However, an error on the collected charge would have the same consequences for both gamma-ray lines. The different deviations obtained for the two lines cannot come from the detector efficiency either, as this quantity is used both for cross section data and for thick target yields, cancelling out in the relation between them. Most probably this difference is a consequence of area extraction. The region 2000–2300 keV is a non-resonance region for the 844 keV line, where, particularly for thin target measurements, this gamma-ray line has a low yield, competing with background lines such as the 847 keV line coming from iron, leading to an area extraction with higher uncertainty.

Some of the resonances found below 1800 keV present energy widths small enough to contradict the conditions imposed by Eq. 1. Therefore, the existing "untrue" cross-sections determined directly from the induced gamma yield need to be replaced by "true" Breit-Wigner resonances [15, 17], for which the determined parameters are given in Table 2 (resonant energies E_R, resonant energy widths Γ_R and the resonant cross-sections σ_R). Breit-Wigner corrections are represented graphically in Fig. 7. Although the corrections are not significant for the analysis of bulk materials, their use is recommended for depth profiling purposes of Al in thin film analysis in order to achieve a better depth sensitivity [27]. It must be highlighted at this point that typically, depth profiling of Al is performed by using the thin and isolated 992 keV resonance of ^{27}Al(p,γ)^{28}Si ($\Gamma_R \approx 0.07$ keV, γ_1—1779 keV) [1, 2, 28]. Nevertheless, for thin film analysis we may perform most of the experiments with appropriate depth resolution

Table 3 Levels of ^{28}Si (not existent in databases) populated by ^{27}Al(p,p'γ)^{27}Al and identified through $\gamma_1 = 844$ keV, $\gamma_2 = 1014$ keV: resonant energies (E_R), energy levels (E-level), energy widths (Γ_R)

Gamma yield	E_R (keV)	E-level (keV)	Γ_R (keV)
844 keV	2366 ± 1	13,866 ± 1	8 ± 1
	2400 ± 1	13,899 ± 1	12 ± 1
1014 keV	2359 ± 1	13,859 ± 1	8 ± 1
	2371 ± 1	13,871 ± 1	11 ± 1
	2393 ± 1	13,892 ± 1	14 ± 1
	2438 ± 2	13,935 ± 2	12 ± 1
Both lines	1961 ± 1	13,475 ± 1	8 ± 1
	2031 ± 1	13,543 ± 1	11 ± 1

The nature of uncertainties is referred in the text

and much higher sensitivity making use of one of the stronger 1683 keV ($\Gamma_R \approx 0.21$ keV) or 1798 keV resonances ($\Gamma_R \approx 0.60$ keV) of the ^{27}Al(p,p'γ)^{27}Al reaction (γ_1—844 keV) [28].

Resonant energies (E_R), half-height widths (Γ_R) and corresponding uncertainties were accurately measured from the experimental excitation functions. Transformation of the resonant data from the laboratory to the centre of mass system was operated, taking into account the energy formation of ^{28}Si by ^{27}Al + p (11,585 keV) [8–10]. ^{28}Si is one of the best studied nuclides, and but even so, some new levels with impact in gamma-ray analysis and not signalized before [8–10], were populated by the inelastic scattering of protons from ^{27}Al, contributing to the first and second excited states of ^{27}Al. Table 3 aggregates the new levels (E-level) found in this work for ^{28}Si (centre of mass system). Aiming future experimental purposes, and for a better comparison with data previously described in nuclear data tables, corresponding values for the incident proton energies (close to the resonant effective energies in the present work) are also presented in Table 3 (in the laboratory system).

4 Conclusions

The excitation functions of the emission lines γ_1—844 keV and γ_2—1014 keV of the ^{27}Al(p,p'γ)^{27}Al nuclear reaction were measured along 268 distinct energy steps in the energy range from 1490 to 3000 keV, resolving deviations of resonant energies previously reported by different authors, also describing in detail their energy profile. In particular, the experiment revealed the presence of strong and very thin resonances below 2.0 MeV, being the γ_1—844 keV emission at the 1683 keV and 1798 keV resonant energies particularly useful for the depth profile of Al in thin films. The cross-section values were validated by calculating induced thick target yields for pure Al at different incident proton beams by using the new excitation function in the ERYA-Bulk code, and by comparing these results with corresponding experimental ones. The calculated yields showed a good agreement with the experimental ones measured in this work and by different authors, promoting the role of PIGE as a standard free analytical technique. Although ^{28}Si is one of the most studied nuclides, the present experiment revealed new energy levels for ^{28}Si not shown in nuclear databases.

Acknowledgements The authors acknowledge LIBPhys (UID/FIS/04559/2019) and NOVA.ID.FCT.

Data availability This manuscript has associated data in a data repository. [Authors' comment: All data included in this manuscript are available upon request by contacting with the corresponding authors.]

References

1. G. Demortier, Non-destructive depth profiling of solid samples by atomic and nuclear interactions induced by charged particles. J. Electron Spectrosc. Relat. Phenom. **129**, 243 (2003). https://doi.org/10.1016/S0368-2048(03)00077-X
2. J.Y. Wang, M. Nastasi (eds.), *Handbook of Modern Ion Beam Materials Analysis*, 2nd edn. (Materials Research Society, Warrendale, USA, 2010)
3. R. Mateus, A.P. Jesus, J.P. Ribeiro, A code for quantitative analysis of light elements in thick samples by PIGE. Nucl. Instrum. Methods Phys. Res. B **229**, 302 (2005). https://doi.org/10.1016/j.nimb.2004.11.019
4. J. Cruz et al., Fluorine depth profiling based on the ^{19}F(p, p'γ)^{19}F excitation function. Eur. Phys. J. Plus **136**, 969 (2021). https://doi.org/10.1140/epjp/s13360-021-01954-3
5. V. Manteigas, L. Martins, J. Cruz, M. Fonseca, A.P. Jesus, ERYA-Bulk and ERYA-profiling: an application for quantitative PIGE analysis. Comput. Phys. Commun. **275**, 108307 (2022). https://doi.org/10.1016/j.cpc.2022.108307
6. I. Zamboni et al., Development of a Reference Database for Particle Induced Gamma Ray Emission (PIGE) Spectroscopy. (IAEA-TECDOC-1822, Vienna, 2017). https://www.iaea.org/publications/12235/. Accessed 1 July 2022
7. IBANDL database, IAEA, http://www-nds.iaea.org/ibandl/. Accessed 1 July 2022
8. National Nuclear Data Center, NNDC, https://www.nndc.bnl.gov/nudat3/. Accessed 1 July 2022
9. Nuclear Data Services, IAEA, https://nds.iaea.org/relnsd/vcharthtml/VChartHTML.html. Accessed 1 July 2022
10. M.S. Basunia, Nuclear data sheets for A = 28. Nucl. Data Sheets **114**, 1189 (2013). https://doi.org/10.1016/j.nds.2013.10.001
11. P.R.P. Allegro, M.A. Rizzutto, N.H. Medina, Improvements in the PIGE technique via gamma-ray angular distribution. Microchem. J. **126**, 287 (2016). https://doi.org/10.1016/j.microc.2015.12.012
12. E. Alves et al., An insider view of the portuguese ion beam laboratory. Eur. Phys. J. Plus **136**, 684 (2021). https://doi.org/10.1140/epjp/s13360-021-01629-z
13. R. Mateus, A.P. Jesus, J. Cruz, J.P. Ribeiro, Measurement of the inelastic scattering of protons by ^{23}Na in the energy range 1.25–2.40 MeV, Nucl. Instrum. Methods Phys. Res. B **219–220**, 307 (2004). https://doi.org/10.1016/j.nimb.2004.01.074

14. M. Chiari et al., Measurement of proton induced γ-ray emission cross sections on Na from 1.0 to 4.1 MeV, Nucl. Instrum. Methods Phys. Res. B **441**, 108 (2019). http://dx.doi.org/https://doi.org/10.1016/j.nimb.2017.01.043
15. A.P. Jesus, B. Braizinha, J. Cruz, J.P. Ribeiro, Influence of target thickness on resonant elastic scattering of protons by ^{19}F. Nucl. Instrum. Methods Phys. Res. B **174**, 229 (2001). https://doi.org/10.1016/S0168-583X(00)00521-8
16. J.F. Ziegler, M.D. Ziegler, J.P. Biersack, SRIM—The stopping and range of ions in matter (2010). Nucl. Inst. Methods Phys. Res. B **268**, 1818 (2010). https://doi.org/10.1016/j.nimb.2010.02.091
17. K. Spyrou, C. Chronidou, S. Harissopulos, S. Kossionides, T. Paradellis, Cross section and resonance strengths of the ^{19}F(p,αγ)^{16}0 reaction in the energy range E_p = 0.8- 3.6 MeV, Z. Phys. A **357**, 283 (1997).
18. A. Jokar et al., Differential cross section measurements of ^{27}Al(p,p′γ) ^{27}Al and ^{27}Al(p,αγ) ^{24}Mg reactions in the energy range of 1.6–3.0 MeV, Nucl. Instrum. Methods Phys. Res. B **362**, 138 (2015). http://dx.doi.org/https://doi.org/10.1016/j.nimb.2015.09.026
19. C. Boni, E. Cereda, G.M.B. Marcazzan, V. de Tomasi, Prompt gamma emission excitation functions for PIGE analysis. Nucl. Instrum. Methods Phys. Res. B **35**, 80 (1988). https://doi.org/10.1016/0168-583X(88)90101-2
20. M. Chiari et al., Measurement of proton induced γ-ray emission cross sections on Al from 2.5 to 4.1 MeV, Nucl. Instrum. Methods Phys. Res. B **332**, 355 (2014). https://doi.org/10.1016/j.nimb.2014.02.095
21. A. Jokar, O. Kakuee, M. Lamehi-Rachti, V. Fathollahi, Thick target yields of proton induced gamma-ray emission from Al, Si and P. Nucl. Instrum. Methods Phys. Res. B **394**, 28 (2017). https://doi.org/10.1016/j.nimb.2016.12.030
22. G. Deconninck, G. Demortier, Quantitative analysis of aluminium by prompt nuclear reactions. J. Radioanal. Chem. **12**, 189 (1972). https://doi.org/10.1007/BF02520988
23. M. Chiari et al., Measurement of proton induced thick target γ-ray yields on B, N, Na, Al and Si from 2.5 to 4.1MeV, Nucl. Instrum. Methods Phys. Res. B **366**, 77 (2016). https://doi.org/10.1016/j.nimb.2015.10.040
24. A.Z. Kiss et al., Measurements of relative thick target yields for PIGE analysis on light elements in the proton energy interval 2.4–4.2 MeV, J. Radioanal. Nucl. Chem. **89**, 123 (1985). https://doi.org/10.1007/BF02070210
25. A. Anttila, R. Hänninen, J. Räisänen, Proton-induced thick-target gamma-ray yields for the elemental analysis of the Z=3–9, 11–21 elements. J. Radioanal. Nucl. Chem. **62**, 293 (1981). https://doi.org/10.1007/BF02517360
26. A. Savidou, X. Aslanoglou, T. Paradellis, M. Pilakouta, Proton induced thick target γ-ray yields of light nuclei at the energy region Ep = 1.0–4.1 MeV, Nucl. Instrum. Methods Phys. Res. B **152**, 12 (1999). https://doi.org/10.1016/S0168-583X(98)00962-8
27. V. Manteigas, J. Cruz, M. Fonseca, A.P. Jesus, ERYA-Profiling: A code for quantitative PIGE analysis of in-depth heterogeneous samples. Nucl. Instrum. Methods Phys. Res. B **502**, 142 (2021). https://doi.org/10.1016/j.nimb.2021.06.006
28. R. Mateus et al., PIGE analysis and profiling of aluminium. Nucl. Instrum. Methods Phys. Res. B **266**, 1490 (2008). https://doi.org/10.1016/j.nimb.2007.11.042